Mean-field modelling of magnetic nanoparticles: The effect of particle size and shape on the Curie temperature

Charles Penny,[1] Adrian R. Muxworthy,[1] and Karl Fabian[2]

[1]*Natural Magnetism Group, Department of Earth Science and Engineering, Imperial College London, London, SW7 2AZ, United Kingdom*

[2]*Geological Survey of Norway, Leiv Eirikssons vei 39, 7491 Trondheim, Norway*

(Received 5 October 2018; revised manuscript received 26 April 2019; published 16 May 2019)

A Heisenberg mean-field model is used to study the effect of size and shape on the Curie temperature of magnetic nanoparticles. Simple cubic, body-centered cubic, and magnetite nanoparticles are modelled as spheres, cubes, and needlelike particles. The Curie temperatures of particles of different shape, but with the same crystal structure and smallest dimension d, are found to differ. The range in the value of the Curie temperature between particles of different shape, ΔT_C, is found to be ~20% of the bulk value of T_C in particles where $d < 10$ atoms. As particle size increases, the value of ΔT_C reduces rapidly and becomes negligible above a threshold size. This threshold size differs between systems and is controlled predominantly by crystal structure. All systems were fit to the finite-size scaling equation, with values of the scaling exponent ν found to lie between 0.46 and 0.55, in good agreement with the expected value of $\nu = 0.5$. No trend in the value of ν due to shape was found.

DOI: 10.1103/PhysRevB.99.174414

I. INTRODUCTION

Interest in magnetic nanoparticles has grown rapidly over the past two decades across a wide range of scientific disciplines: applications in magnetic hyperthermia treatment [1], improved contrast agents for MRI imaging [2], and heat-assisted magnetic recording [3] are all actively being pursued. In the environment, magnetic nanoparticles have been proposed as the source of magnetic anomalies over oil fields [4], and their presence in the human brain due to inhalation of anthropogenic pollution has recently been linked to Alzheimer's disease and other neurodegenerative diseases [5]. Despite this interest there are still several fundamental unanswered questions surrounding the magnetic behavior of nanoparticles and other nanoscale structures. Many of these questions arise from a combination of interacting phenomena, making it no longer possible to simply use the bulk parameters to describe the magnetic nanoparticles' behavior.

In bulk magnetic systems, the spin correlation length diverges at the Curie temperature T_C, but in nanoscale systems the growth of the correlation length is limited by the smallest dimension of the system such that it causes a reduction in T_C. This obeys a finite-size scaling relationship [6],

$$\frac{T_C(\infty) - T_C(d)}{T_C(\infty)} = \left(\frac{d_0}{d}\right)^{\frac{1}{\nu}}, \tag{1}$$

where $T_C(\infty)$ is the bulk Curie temperature, d_0 is a characteristic length scale of the system, ν is the correlation length scaling exponent, and d is the smallest length scale of the system. Recent developments in preparation techniques have lead to several new experimental investigations of finite-sized scaling in magnetic nanoparticles. However, the results have been varied in contrast with the good agreement between theory and experiment found in studies of thin films [7,8]. Studies of hematite and magnetite nanoparticles have found values for ν in the range of 0.6–0.8 [9,10], close to the expected value of 0.7043 [11] for the 3D Heisenberg model. A value of $\nu = 1.06$ was determined from work conducted on Ni nanoparticles [12], with line dislocations near the surface of the nanoparticles suggested as the cause of this discrepancy.

Monte Carlo modelling of nanoscale systems has failed to clarify the situation, with values of ν derived from finite-size scaling also failing to agree with the accepted value of the correlation length scaling exponent. An Ising Monte Carlo simulation of maghemite nanoparticles suggested a value of $\nu = 0.49$ from finite sized scaling [13], in clear disagreement with the 3D Ising value of 0.6417 calculated from consideration of thermodynamic derivatives [14]. Simulations of $L1_0$-FePt using a classical-spin Heisenberg model determined a value of $\nu = 1.06$ [15], again disagreeing with the generally accepted value. Long-range ordering was suggested as a possible source of this disagreement.

Here we use an atomistic mean-field model based on an approach previously used for analyzing complex magnetic structures [16] and apply it to nanoscale systems. The model was applied to a number of crystal structures; simple synthetic systems with uniform spin and exchange energies and a model of magnetite (Fe_3O_4). The effect of shape on the Curie temperature of magnetic nanoparticles was studied and finite-size scaling in these systems considered.

II. MEAN-FIELD MODELLING OF MAGNETIC NANOPARTICLES

The mean-field approximation is a well understood method for analyzing the behavior of magnetic systems, having been successfully applied across the spectrum of magnetic models from the Ising model to spin glasses [17,18]. The generalized mean-field equations for a system of interacting Heisenberg

spins are given by

$$m_i = B_{S_i}\left(S_i \frac{\sum_{j\in N_i} 2J_{ij}S_j m_j + g\mu_B h}{k_B T}\right), \quad (2)$$

where m_i is the normalized magnetization of site i, S_i is the spin at site i, B_{S_i} is the Brillouin function, J_{ij} is the isotropic exchange interaction between sites i and j defined such that ferromagnetic exchange is positive, $g \approx 2$ is the gyromagnetic ratio, μ_B is the Bohr magneton, h is an external magnetic field acting on each site, k_B is the Boltzmann constant, and T is temperature. The sum over j acts over the set of nearest neighbors of i, where $N_i := \{j : J_{ij} \neq 0\}$. Each site i is a spin in the system being studied and so can represent the unique atoms in a complex crystal lattice [16], the layers in a thin film [19], or as in the case being studied here, the atoms in a magnetic nanoparticle. A full derivation of the mean-field equations is given in Appendix A.

The mean-field equations in the form of (2) are a system of N coupled nonlinear equations. Because its solution is not analytically tractable, a numerical approach must be taken. By recasting (2) as

$$f_i = B_{S_i}\left(S_i \frac{\sum_{j\in N_i} 2J_{ij}S_j m_j + g\mu_B h}{k_B T}\right) - m_i = 0, \quad (3)$$

the problem is transformed to finding a common zero of the set of expressions f_i. There is normally more than a single solution to such systems of equations, and so further conditions must be fulfilled by the desired solution. In the case of the mean-field equations, the trivial root $m_i = 0$ is not a valid solution below T_C, when it falls at a maximum of free energy. In addition, m_i are normalized magnetic moments; they all must lie in the range $-1 \leqslant m_i \leqslant 1$.

The system of equations described by (3) was solved by a C++ program using the SNES solvers of the Portable, Extensible Toolkit for Scientific Computation (PETSc) libraries [20]. PETSc uses N-dimensional Newton based methods that require either an analytic expression or a finite-difference approximation of the Jacobian ($\frac{\partial f_i}{\partial m_j}$) to iteratively solve systems of nonlinear equations. In the case of (3), an analytic expression for the Jacobian can be obtained. For $i = j$,

$$\frac{\partial f_i}{\partial m_i} = -1. \quad (4)$$

For $j \in N_i$,

$$\frac{\partial f_i}{\partial m_j} = \frac{2J_{ij}S_j}{k_B T}\left[\left(\frac{1}{2S_i}\right)^2 \frac{1}{\sinh^2\left(\frac{1}{2S_i}\xi_i\right)} - \left(\frac{2S_i+1}{2S_i}\right)^2 \frac{1}{\sinh^2\left(\frac{2S_i+1}{2S_i}\xi_i\right)}\right], \quad (5)$$

where

$$\xi_i = \frac{\sum_{j\in N_i} 2J_{ij}\langle S_j\rangle + g\mu_B h}{k_B T}. \quad (6)$$

Otherwise for $i \neq j$ and $j \notin N_i$,

$$\frac{\partial f_i}{\partial m_j} = 0. \quad (7)$$

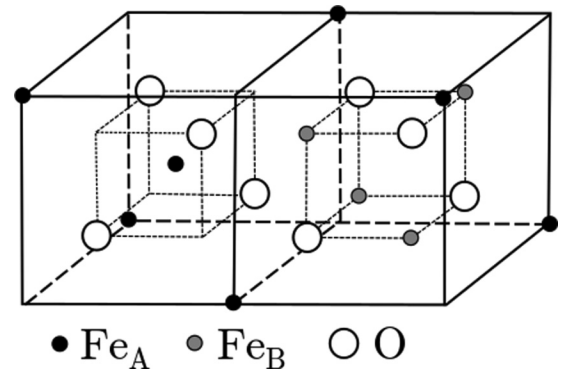

FIG. 1. Structure of magnetite showing two octants of the unit cell. The octants are arranged in a chess board pattern to form the unit cell.

A. Crystal structures and particle shapes

Particles were modelled using simple cubic, body-centered cubic, and inverse spinel (magnetite) crystal structures. For each crystal structure, five different shapes were studied: cubes, spheres, and three elongated needlelike shapes with aspect ratios of 2:1:1, 5:1:1, and 10:1:1. Each shape was modelled over a range of sizes (see Table I). Spherical particles were approximated on the crystal lattice by including an atom if it lay within $\frac{d}{2}$ of the center of the particle.

Simple cubic (sc) and body-centred cubic (bcc) particles were modelled with an isotropic spin of $S = 2$ applied to each atom, and a ferromagnetic exchange energy of $J = 3.5\,k_B \approx 0.3$ meV between each nearest neighbor.

We also considered magnetite (Fe_3O_4), as it is an important and well understood natural mineral, which forms in the inverse spinel structure (Fig. 1). 32 oxygen (O^{2-}) atoms form a face centered cubic lattice, with 24 iron atoms occupying tetrahedral (A) and octahedral (B) interstitial sites. Eight Fe^{3+} atoms occupy the A sites, while the 16 B sites are occupied by an equal number of randomly distributed Fe^{3+} and Fe^{2+} ions [21]. The magnetic structure of magnetite is ferrimagnetic, with the magnetic moments of the A and B sites aligned in opposing directions. The total theoretical moment of magnetite is 4 μ_B per formula weight, in close agreement with the experimentally determined value of 4.1 μ_B [22].

For the model of magnetite, spins of $S_A = 2.5$ and $S_B = 2.25$ were assigned to the A and B sites. Nearest-neighbor exchange energies of $J_{AA} = -1.56$ meV, $J_{AB} = -2.38$ meV, and $J_{BB} = 0.26$ meV were used as the most complete set of experimental estimations [23].

B. Determining the Curie temperature

Previous studies determined the Curie temperature by linearizing the Brillouin function in Eq. (2) and then solving the arising matrix equation for the case of a singular matrix [16]. This approach rapidly became too expensive here given the large number of unique sites even in small particles and so an alternative approach was used.

The solution of the mean-field equations gives the magnetization of each atom in the particle for a given temperature T. Below T_C, this gives a nonzero value of magnetization for each

TABLE I. Range of smallest length scales, d, for all particles modelled in terms of number of atoms. Not all particle diameters in the range were calculated. For inverse spinel systems, particle sizes are also listed in nm for the case of magnetite.

			Needle		
	Cube	Sphere	2:1:1	5:1:1	10:1:1
Simple cubic	2–45	3–50	2–40	2–24	2–19
Body-centered cubic	3–67	5–67	3–41	3–37	3–29
	8–104	8–120	8–76	8–56	8–44
Inverse spinel	0.84–10.92 nm	0.84–12.60 nm	0.84–7.98 nm	0.84–5.88 nm	0.84–4.62 nm

site; for $T \geqslant T_C$, magnetization at each site is zero. It is therefore possible to determine T_C by a bisection algorithm. Two initial temperatures were chosen, $T_L = 1$ K and $T_H > T_C(\infty)$. The magnitude of the average magnetization of the particle, $|\langle m_i \rangle|$, at the midpoint between these two temperatures,

$$T_M = \frac{T_L + T_H}{2}, \tag{8}$$

was calculated. If at this temperature $|\langle m_i \rangle|$ was found to be greater than a threshold value $\epsilon_m = 0.0001$, then T_M was assumed to be below the Curie temperature, and T_L was replaced by T_M. For $|\langle m_i \rangle| < \epsilon_m$, T_H was replaced by T_M. This process was iterated, until $T_H - T_L < 0.01$ K. The Curie temperature of the particle was then taken as

$$T_C = \frac{T_{L_f} + T_{H_f}}{2}, \tag{9}$$

where T_{L_f} and T_{H_f} are the final values of T_L and T_H, respectively, and the error in T_C is

$$\epsilon_{\text{err}} = \frac{T_{L_f} - T_{H_f}}{2}. \tag{10}$$

Excellent agreement in the value of T_C between the two methods, typically better than 0.02 K, was found in small simple cubic systems.

III. RESULTS AND DISCUSSION

A. Properties of nanoparticles

Normalized magnetization curves, $m(T)$, were calculated in steps of $\Delta T = 0.1$ K for bcc and sc particles, and $\Delta T = 1$ K for magnetite particles. A sharp Curie-temperature phase transition can be seen for all particles, with the Curie temperature decreasing with decreasing particle size (Fig. 2). In real systems of this size, identifying the Curie temperature is more complex; the superparamagnetic nature of many magnetic nanoparticles requires measurements to be made in the presence of an external field, which destroys the second-order phase transition, while samples will inevitably contain a distribution of grain sizes and morphologies [24].

The very smallest bcc (not shown) and the magnetite particles have more 'linear' m-T curves than larger particles of the same crystal structure. Their behavior is strongly influenced by atoms in the corner of the cubes, which have only one or two nearest neighbors.

Magnetization varies spatially throughout the nanoparticles at all temperatures (Fig. 3). At low temperatures, a core-shell-like structure is seen, in which a core of atoms behaves in a bulklike manner, surrounded by a shell of atoms exhibiting reduced magnetization. As the temperature increases, this boundary softens, and there is a more gradual change in magnetization throughout the particle. This behavior has previously been observed [25].

B. Effect of varying particle shape

The Curie temperature of small magnetic nanoparticles is affected by the shape of the particle (Fig. 4). Spherical particles have the lowest Curie temperature for a given size, d, with cubic, 2:1:1, 5:1:1, and 10:1:1 particles having successively higher values of T_C.

It should be noted that the number of atoms in a 10:1:1 particle of size d is an order of magnitude higher than a spherical or cubic particle of the same size. If T_C of a 10:1:1 particle is compared to that of a spherical particle containing the same number of atoms (thus larger d), the sphere has the highest Curie temperature. This is due to the more compact shape of a sphere, which leads to both fewer atoms on the surface and a greater average distance from the surface for atoms inside the sphere.

The normalized difference in the Curie temperature between spherical and 10:1:1 particles is defined as

$$\Delta T_C(d) = \frac{T_{C_{10:1:1}}(d) - T_{C_{\text{sph}}}(d)}{T_C(\infty)} \tag{11}$$

and is used as a measure of the strength of the influence of shape on T_C. In the smallest particles, ΔT_C is found to be

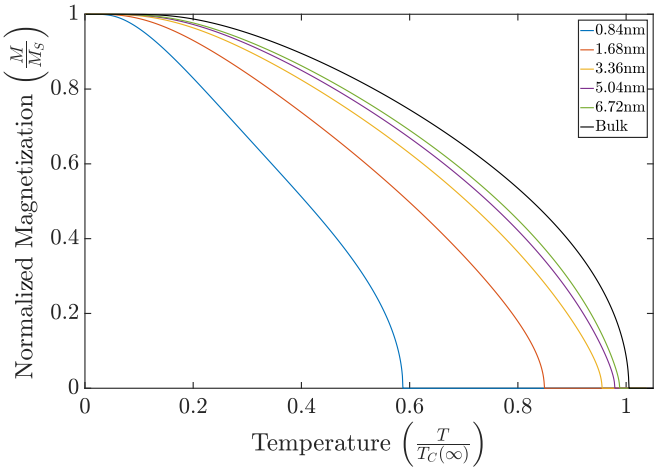

FIG. 2. Magnetization curves of cubic magnetite particles of a number of different sizes. The bulk mean-field magnetization curve is included for reference. Particle sizes are given in nm.

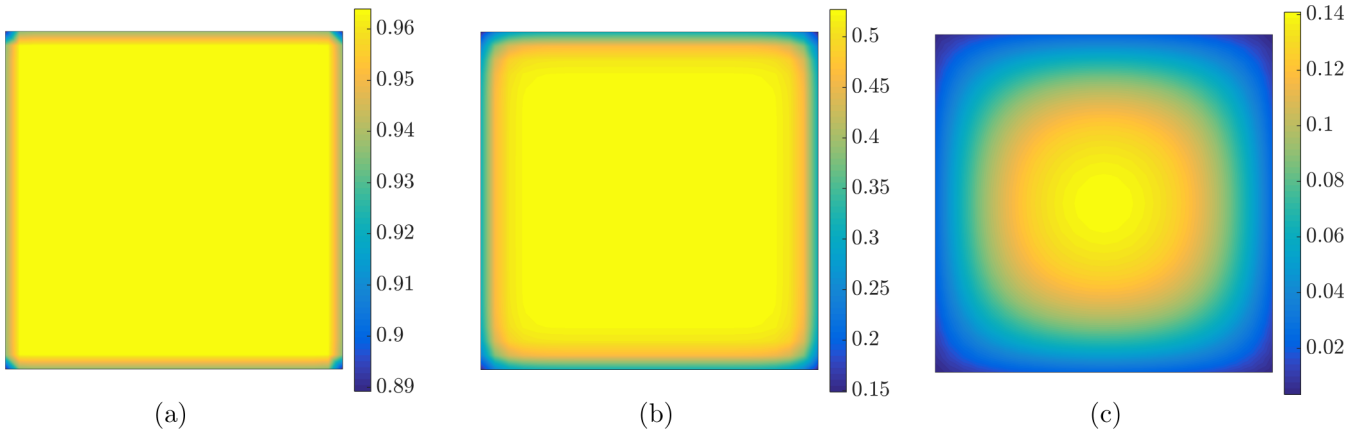

FIG. 3. Variation of magnetization in a cube of 25 × 25 × 25 atoms arranged in a simple cubic lattice. A slice through the middle of the particle at $z = 13$ is shown at three different normalized temperatures: (a) $t = 0.36$, (b) $t = 0.87$, (c) $t = 0.99$, where $t = \frac{T}{T_C(d)}$.

15–25% of $T_C(\infty)$ before it falls off rapidly as particle size increases [Fig. 5(a)]. The size at which ΔT_C become negligible (taken as $\Delta T_C < 0.02$) varies between crystal structures. In simple cubic and bcc particles this occurs as a size of 10 and 20 atoms, respectively. For magnetite, our results suggest that shape is only an important factor in particles smaller than 5 nm (≈50 atoms) in size.

The sensitivity of ΔT_C with respect to the relative magnitudes of exchange energy was tested in magnetite [Fig. 5(c)]. Two additional sets of calculations were made, one using estimations of exchange energies from *ab initio* calculations [26] and another using uniform values of $J = 3.5k_B$. The latter choice creates an artificial ferromagnetic system, with the value of J selected to match the other systems modelled in this work. For all particle sizes, except for the smallest size $d = 0.8$ nm, the value of ΔT_C does not change appreciably as exchange energies differ. When $d = 0.8$ nm, a small difference in the value of ΔT_C of 0.05 was seen between the ferromagnetic and two ferrimagnetic systems. This suggests that the relative magnitudes of exchange energies have little bearing on the value of ΔT_C and that the size below which shape begins to have an impact on the Curie temperature is controlled predominantly by crystal structure.

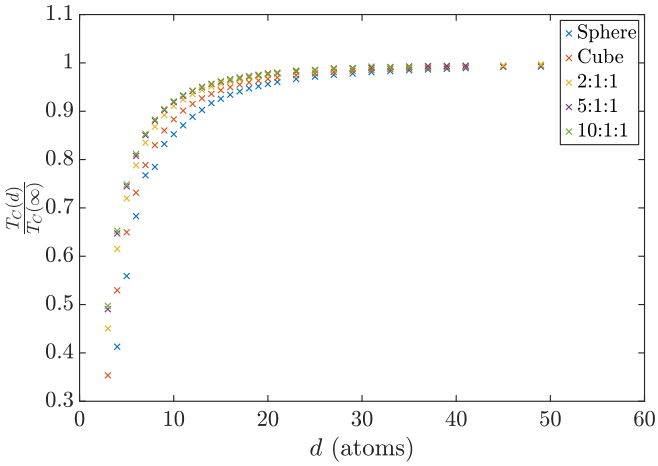

FIG. 4. Normalized Curie temperature of bcc nanoparticles. Data for five shapes is shown: spherical, cubic, 2:1:1, 5:1:1, and 10:1:1 particles.

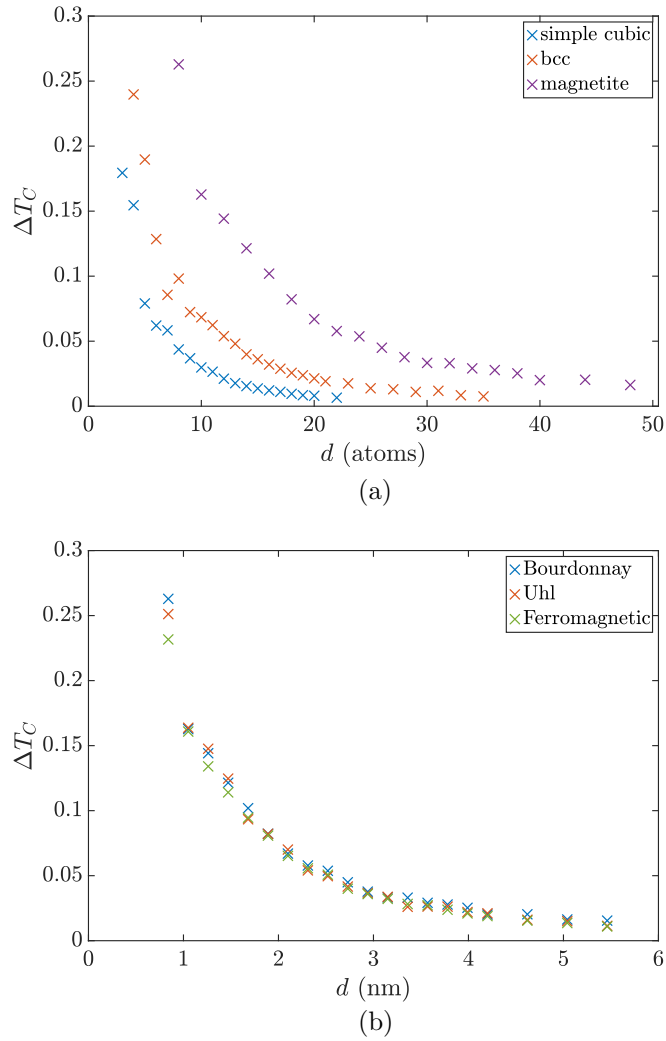

FIG. 5. ΔT_C as a function of d. (a) Illustrates the effect of variation due to crystal structure. (b) Illustrates the effect of changes to exchange energy in magnetite between experiment [23], *ab initio* modelling [26], and an artificial ferromagnetic system.

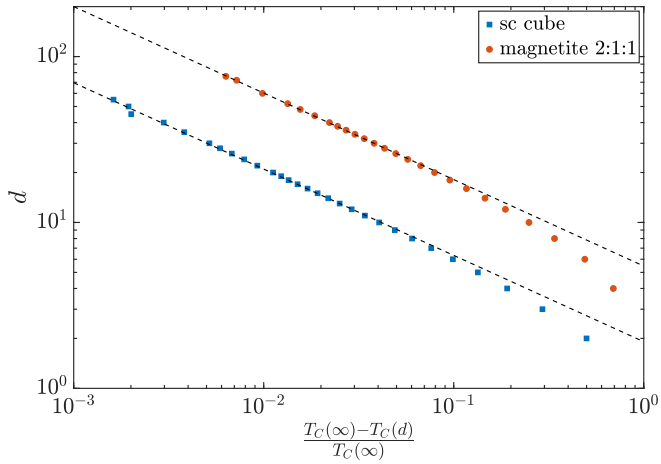

FIG. 6. Example fits to determine the value of the scaling exponent ν for cubic sc and magnetite 2:1:1 particles. The dashed lines show the best fits to Eq. (1) where the error in ν is minimized.

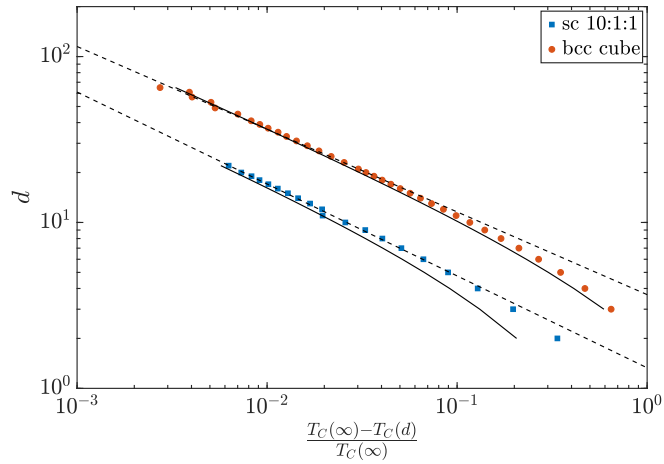

FIG. 8. Comparison of the finite-size scaling law (1), and the modified scaling law (12) in cubic bcc and simple cubic 10:1:1 particles. The solid lines show the analytical results from (12). The dashed lines show the best fit to Eq. (1) where the error in ν is minimized.

C. Finite-size scaling

Values for the scaling exponent ν were calculated by nonlinear least squares regression to Eq. (1) using the Levenberg-Marquardt algorithm [27]. The error in ν was taken as the 95% confidence interval of the best fit value. Particles of different materials and shapes were considered separately. Fitting was undertaken initially on all sizes of particles from a particular system and then successively removing the smallest particle from the fit. The final value of ν was taken as the one with the smallest error, in order to account for any deviation from scaling behavior seen at small sizes.

The chosen fits describe much of the data well, with deviation away from scaling behavior for diameters smaller than $d \approx 10$ atoms for simple cubic systems, $d \approx 15$ atoms for bcc systems, and $d \approx 20$ atoms for magnetite systems (examples of fitting shown in Fig. 6). Values of ν are close to the analytical mean-field result of $\nu = 0.5$ [28] in all cases, lying in the range 0.46–0.55 (Fig. 7). No trend in the value of the scaling exponent with respect to particle shape can be seen. This consistency of results close to the accepted value of the scaling exponent contrasts with the range of values of ν found in other studies [9,10,12,15].

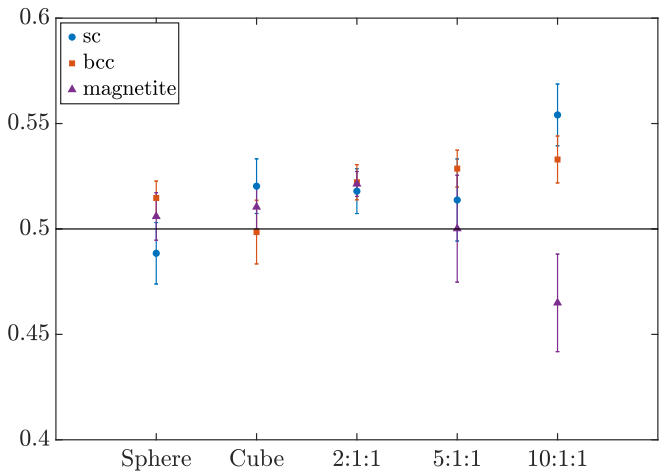

FIG. 7. Calculated values of ν for simple cubic, bcc, and magnetite systems. Errors donate 95% confidence interval of the fit. Solid line highlights the analytical mean-field value of $\nu = 0.5$.

An analytical expression for the Curie temperature of some types of nanoparticle has been derived from Ginzberg-Landau (G-L) theory [25]. This approach has been applied to cubic and long needle particles of simple cubic, body centered cubic, and face centered cubic structure. A modified scaling law is predicted in which

$$\frac{T_C(\infty) - T_C(d)}{T_C(\infty)} = \kappa \left(\frac{\pi}{d+2} \right)^2, \tag{12}$$

where κ depends upon the shape and crystal structure of the particle. For a simple cubic structure, $\kappa = \frac{1}{2}$ for a cubic particle and $\kappa = \frac{1}{3}$ for a long needle. For a body centered cubic structure, $\kappa = \frac{3}{2}$ for a cubic particle and $\kappa = 1$ for a long needle.

The difference in Curie temperature between 5:1:1 and 10:1:1 particles in the mean-field model is very small (Fig. 4), suggesting that the 10:1:1 particle is a good approximation to a long needle. We can therefore directly compare the analytical result above with the results from the mean-field model. The G-L theory clearly captures the deviation away from finite-size scaling seen in the mean-field approach at very small length scales (Fig. 8). However, the quantitative agreement between the two models varies. For cubic bcc particles, the two models agree very closely, but for simple cubic 10:1:1 particles a larger difference in predictions can be seen; G-L theory predicts a value of T_C approximately half of the value of mean-field theory for the smallest systems.

The qualitative accuracy of the modified scaling law was tested by fitting the mean-field data to a law of the general form of (12),

$$\frac{T_C(\infty) - T_C(d)}{T_C(\infty)} = \left(\frac{d_0}{d+2} \right)^{\frac{1}{\nu}}. \tag{13}$$

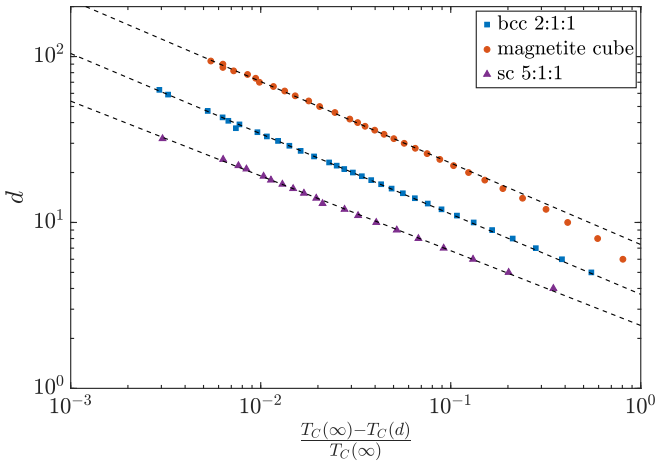

FIG. 9. Example fits to the general modified scaling law (13) for bcc 2:1:1, cubic magnetite, and sc 5:1:1 particles. The dashed lines show the best fits to Eq. (13) where all particles are included in the fit.

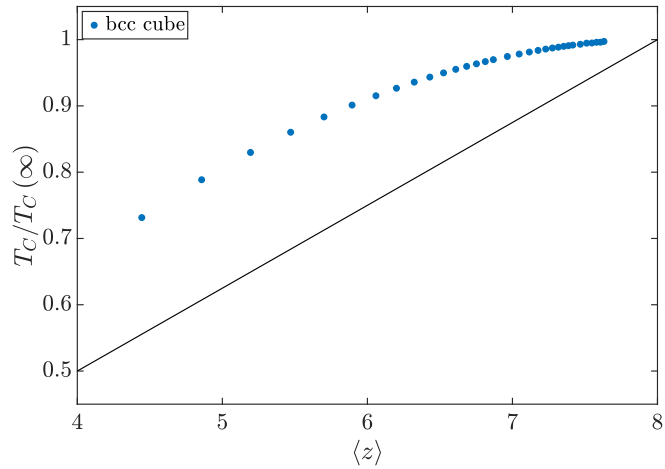

FIG. 10. Plot of reduced Curie temperature against average coordination number for bcc nanoparticles. The solid line shows the linear relationship suggested in (15). No agreement between this relationship and the numerical results can be seen.

In contrast to the fitting procedure for finding ν used earlier, only a single fit of all data points was made in order to test (13) across all length scales. The results for simple cubic and bcc particles show that the general form of the modified law describes the scaling behavior at small length scales well (Fig. 9). However, for magnetite particles, Eq. (13) does not describe the scaling behavior at small length scales, with deviation away from this law clearly seen. We suggest this is due to the complex crystal structure of magnetite which involves interactions over many layers of the unit cell. This is in contrast to the simpler sc, bcc, and fcc ordering, which only interact with neighbors in adjacent layers, for which Eq. (12) is derived.

D. Coordination number

In the bulk mean-field Heisenberg model the Curie temperature, $T_C(\infty)$, is described to a good linear approximation by

$$T_C(\infty) = \frac{(S+1)}{3S}\frac{2zJS^2}{k_B}, \tag{14}$$

where S is the isotropic spin, z is the number of nearest neighbors, and J is the isotropic exchange energy. In the bulk case, the Curie temperature is linearly dependent on the number of nearest neighbors in the system, assuming all other variables are held constant. In view of the relationship between T_C and z in (14), it may seem reasonable to assume that $T_C(d)$ can be described to a good approximation by the average coordination number $\langle z \rangle$,

$$T_C(d) = \frac{(S+1)}{3S}\frac{2\langle z\rangle JS^2}{k_B}. \tag{15}$$

By considering the left hand side of the scaling Eq. (1), and substituting in Eqs. (14) and (15), an expression for scaling as a function of average coordination number is then obtained,

$$t = \frac{T_C(\infty)-T_C(d)}{T_C(\infty)} = 1 - \frac{\langle z\rangle}{z}. \tag{16}$$

Analytic expressions for $\langle z \rangle$ in cubic sc and bcc particles can be found and are given by

$$\langle z_{\rm sc}\rangle = 6 - \frac{6}{d} \tag{17}$$

and

$$\langle z_{\rm bcc}\rangle = \frac{4(2d^3 - 6d^2 + 6d + 8)}{d(d^2+3)}. \tag{18}$$

By further substituting in the expressions for $\langle z_{\rm sc}\rangle$ and $\langle z_{\rm bcc}\rangle$ into (16) expressions for $t_{\rm sc}$ and $t_{\rm bcc}$ in terms of d are obtained. For a simple cubic system, where $z = 6$,

$$\frac{T_C(\infty)-T_C(d)}{T_C(\infty)} = 1 - \left(\frac{6-\frac{6}{d}}{6}\right) = \frac{1}{d}, \tag{19}$$

which is a power law of the form in Eq. (1) where $\nu = 1$ and $d_0 = 1$. For a bcc system, where $z = 8$,

$$\frac{T_C(\infty)-T_C(d)}{T_C(\infty)} = 1 - \frac{\left(2 - \frac{6}{d} + \frac{6}{d^2} + \frac{8}{d^3}\right)}{2 + \frac{6}{d^2}}. \tag{20}$$

The d^{-2} and d^{-3} terms quickly become small compared to the d^{-1} term, and so,

$$\frac{T_C(\infty)-T_C(d)}{T_C(\infty)} \to 1 - \left(\frac{2-\frac{6}{d}}{2}\right) = \frac{3}{d}, \tag{21}$$

which again recovers a power law where $\nu = 1$ (and $d_0 = 3$). This result is in clear contrast to the mean-field value of $\nu = 0.5$ and shows that the assumption made in (15) does not hold in the mean-field approximation (also shown in Fig. 10). A previous study of magnetic nanoparticles using the free-energy variational principle found that the expression in (16) was true to a first approximation in that model [29]. The value for the scaling exponent obtained by the variational method for both bcc and fcc lattices was found to be

$\nu = 1.0001 \pm 0.0001$, in agreement with the result obtained above.

IV. CONCLUSIONS

This study has used the mean-field approximation applied to finite systems of Heisenberg spins to investigate the particle size and shape dependence on the Curie temperature of magnetic nanoparticles. A numerical model was developed to solve the generalized mean-field equations for a number of particle shapes and crystal structures.

T_C was found to vary between different shapes of particle, with spheres, cubes, 2:1:1, 5:1:1, and 10:1:1 particles having successively higher values of Curie temperature for the same smallest dimension. ΔT_C, the difference in Curie temperature between 10:1:1 and spherical particles, was found to be 15–25% of the value of $T_C(\infty)$ in particles a few atoms across and rapidly decreased as particle size increased. The size at which ΔT_C became negligible was found to differ between crystal structures. For magnetite this was found to be 5 nm. ΔT_C was also found to be insensitive to changes in the exchange energy between neighboring atoms, showing that crystal structure is the primary driver of the differences in T_C due to shape.

All systems were fit to the finite-size scaling law and a good fit was found in all cases. Very small particles, typically $d < 10$–20 atoms, showed deviation away from finite-size scaling behavior. Values of ν were found to lie in the range 0.46–0.55, which compare well to the analytical mean-field value of 0.5. No trend in the value of ν with relation to particle shape was found. A modified scaling law, derived from Ginzberg-Landau theory, accounted for the observed deviation from finite-size scaling in simple cubic and bcc particles, but was not successful when applied to magnetite.

ACKNOWLEDGMENTS

C.P. was supported through both the UK STFC (ST/N504312/1) and a studentship in the Centre for Doctoral Training on Theory and Simulation of Materials at Imperial College London funded by the EPSRC (EP/L015579/1). A.R.M. acknowledges the support of UK STFC (Grant No. ST/J001260/1).

APPENDIX: DERIVATION OF MEAN-FIELD EQUATIONS

The derivation presented here applies the mean-field approximation to finite systems of spins in three spatial dimensions; it is closely related to work conducted previously [16] but restricts the spin orientations and the applied field to lie in one direction. However, the final set of equations here features a factor of S_i inside the Brillouin function which is not present in the former work. This discrepancy arises between (A16) and (A20), which is treated as a single step in the previous work, and so a full treatment is given here for clarity.

The Heisenberg Hamiltonian for a system of N magnetic spins considering exchange and external field h is given by [28]

$$\mathcal{H} = -2\sum_{\langle ij\rangle} J_{ij}S_iS_j - g\mu_B h\sum_{i=1}^{N} S_i, \tag{A1}$$

where S_i is the spin of site i, J_{ij} is the isotropic exchange energy ($J_{ij} = J_{ji}$) between sites i and j, $g \approx 2$ is the gyromagnetic ratio, μ_B is the Bohr magneton, and h is an external field acting on each site. The sum over $\langle ij\rangle$ is over nearest neighbor pairs. The definition of the Heisenberg Hamiltonian here gives a positive value to ferromagnetic and a negative value to antiferromagnetic exchange energies. The sum of the first term is taken over each nearest neighbor pair of sites and may be rewritten as

$$\mathcal{H} = -\sum_{i=1}^{N}\sum_{j\in N_i} J_{ij}S_iS_j - g\mu_B h\sum_{i=1}^{N} S_i, \tag{A2}$$

where N_i is the set of nearest neighbor spins of site i.

The temporal fluctuation δ_i of the ith spin is defined as [18]

$$\delta_i = S_i - \langle S_i\rangle, \tag{A3}$$

where $\langle S_i\rangle$ is the average value or magnetization of spin i. The Hamiltonian in terms of δ_i may be written as

$$\mathcal{H} = -\sum_{i=1}^{N}\sum_{j\in N_i} J_{ij}(\delta_i\delta_j + \delta_i\langle S_j\rangle + \langle S_i\rangle\delta_j + \langle S_i\rangle\langle S_j\rangle) - g\mu_B h\sum_{i=1}^{N} S_i. \tag{A4}$$

The mean-field approximation is taken, in which correlations between fluctuations are neglected (i.e., $\delta_i\delta_j = 0$) [18]. This gives the mean-field Hamiltonian,

$$\mathcal{H}_{\mathrm{MF}} = -\sum_{i=1}^{N}\sum_{j\in N_i} J_{ij}(\delta_i\langle S_j\rangle + \langle S_i\rangle\delta_j + \langle S_i\rangle\langle S_j\rangle) - g\mu_B h\sum_{i=1}^{N} S_i. \tag{A5}$$

Substitution of Eq. (A3) and summation over all sites allows simplification to

$$\mathcal{H}_{\mathrm{MF}} = \sum_{i=1}^{N}\sum_{j\in N_i} J_{ij}(\langle S_i\rangle\langle S_j\rangle - 2S_i\langle S_j\rangle) - g\mu_B h\sum_{i=1}^{N} S_i. \tag{A6}$$

In order to find the equilibrium state of the system, the minimum of the free energy must be found. The free energy F is given in terms of the well known equation $F = -k_BT\ln Z$ where Z is the partition function. The partition function is given by the expression

$$Z = \sum_{\{S_i\}} \exp\left(\frac{-\mathcal{H}}{k_BT}\right), \tag{A7}$$

where $\{S_i\}$ is the sum over all possible states of the system defined by $\mathcal{H}$. Substitution of (A6) and the quantization of angular momentum yields the following expression for the partition function,

$$Z = \exp\left(-\sum_{i=1}^{N}\sum_{j\in N_i}\frac{J_{ij}\langle S_i\rangle\langle S_j\rangle}{k_BT}\right)\prod_{i=1}^{N}\sum_{\sigma=-S_i}^{S_i}\exp(\xi_i\sigma), \tag{A8}$$

where

$$\xi_i = \frac{\sum_{j\in N_i} 2J_{ij}\langle S_j\rangle + g\mu_B h}{k_B T}. \tag{A9}$$

Noting the geometric series summation, a final expression for Z is given by

$$Z = \exp\left(-\sum_{i=1}^{N}\sum_{j\in N_i}\frac{J_{ij}\langle S_i\rangle\langle S_j\rangle}{k_B T}\right)\prod_{i=1}^{N}\frac{\sinh\left(\frac{2S_i+1}{2}\xi_i\right)}{\sinh\left(\frac{1}{2}\xi_i\right)}. \tag{A10}$$

The free energy can be calculated by direct substitution,

$$F = \sum_{i=1}^{N}\sum_{j\in N_i} J_{ij}\langle S_i\rangle\langle S_j\rangle - k_B T\sum_{i=1}^{N}\ln\frac{\sinh\left(\frac{2S_i+1}{2}\xi_i\right)}{\sinh\left(\frac{1}{2}\xi_i\right)} = F_1 - F_2. \tag{A11}$$

The equilibrium state of the system occurs when the derivative of free energy with respect to each magnetization, $\frac{\partial F}{\partial\langle S_i\rangle} = 0$. The two terms of the free energy are considered separately,

$$F_1 = \sum_{i=1}^{N}\sum_{j\in N_i} J_{ij}\langle S_i\rangle\langle S_j\rangle, \tag{A12}$$

and

$$F_2 = k_B T\sum_{i=1}^{N}\ln\frac{\sinh\left(\frac{2S_i+1}{2}\xi_i\right)}{\sinh\left(\frac{1}{2}\xi_i\right)}. \tag{A13}$$

The partial derivative of F_1 yields

$$\frac{\partial F_1}{\partial\langle S_i\rangle} = \sum_{j\in N_i} 2J_{ij}\langle S_j\rangle, \tag{A14}$$

where the factor of two arises from the sum over all sites. The case of F_2 requires a little more manipulation but finally obtains the expression

$$\frac{\partial F_2}{\partial\langle S_i\rangle} = \sum_{j\in N_i} 2J_{ij}\left[\frac{2S_j+1}{2}\coth\left(\frac{2S_j+1}{2}\xi_j\right) - \frac{1}{2}\coth\left(\frac{1}{2}\xi_j\right)\right], \tag{A15}$$

which is related to the Brillouin function by

$$\frac{\partial F_2}{\partial\langle S_i\rangle} = \sum_{j\in N_i} 2J_{ij}S_j B_{S_j}(S_j\,\xi_j), \tag{A16}$$

or equivalently

$$\frac{\partial F_2}{\partial\langle S_i\rangle} = \sum_{j\in N_i} 2J_{ij}S_j B_{S_j}\left(S_j\frac{\sum_{k\in N_j} 2J_{jk}\langle S_k\rangle + g\mu_B h}{k_B T}\right). \tag{A17}$$

The sum over j is a summation over the nearest neighbors of site i, while the sum over k is a sum over the nearest neighbors of site j. A minimum of free energy is therefore found when

$$\frac{\partial F}{\partial\langle S_i\rangle} = \sum_{j\in N_i} 2J_{ij}\left[\langle S_j\rangle - S_j B_{S_j}(S_j\xi_j)\right] = 0. \tag{A18}$$

Each term in the sum must equal zero to prevent solutions featuring the self interaction of spins, and so the solution to (A18) reduces to N coupled equations,

$$\langle S_i\rangle = S_i B_{S_i}\left(S_i\frac{\sum_{j\in N_i} 2J_{ij}\langle S_j\rangle + g\mu_B h}{k_B T}\right). \tag{A19}$$

By defining the site normalized magnetization $m_i = \frac{\langle S_i\rangle}{S_i}$, the final form of (A19) is

$$m_i = B_{S_i}\left(S_i\frac{\sum_{j\in N_i} 2J_{ij}S_j m_j + g\mu_B h}{k_B T}\right). \tag{A20}$$

[1] M. Johannsen, B. Thiesen, P. Wust, and A. Jordan, Int. J. Hyperth. **26**, 790 (2010).

[2] L. M. Parkes, R. Hodgson, L. T. Lu, L. D. Tung, I. Robinson, D. G. Fernig, and N. T. K. Thanh, Contrast Media Mol. Imaging **3**, 150 (2008).

[3] D. Weller, O. Mosendz, G. Parker, S. Pisana, and T. S. Santos, Phys. Status Solidi A **210**, 1245 (2013).

[4] R. Abubakar, A. R. Muxworthy, M. A. Sephton, P. Southern, J. S. Watson, A. Fraser, and T. P. Almeida, Mar. Pet. Geol. **68**, 509 (2015).

[5] B. A. Maher, I. A. M. Ahmed, V. Karloukovski, D. A. MacLaren, P. G. Foulds, D. Allsop, D. M. A. Mann, R. Torres-Jardón, and L. Calderon-Garciduenas, Proc. Natl. Acad. Sci. USA **113**, 10797 (2016).

[6] M. E. Fisher and A. E. Ferdinand, Phys. Rev. Lett. **19**, 169 (1967).

[7] F. Huang, G. J. Mankey, M. T. Kief, and R. F. Willis, J. Appl. Phys. **73**, 6760 (1993).

[8] T. Ambrose and C. L. Chien, Phys. Rev. Lett. **76**, 1743 (1996).

[9] L. Li, F. Li, J. Wang, and G. M. Zhao, J. Appl. Phys. **116**, 174301 (2014).

[10] J. Wang, W. Wu, F. Zhao, and G. M. Zhao, Appl. Phys. Lett. **98**, 083107 (2011).

[11] K. Chen, A. M. Ferrenberg, and D. P. Landau, Phys. Rev. B **48**, 3249 (1993).

[12] J. Wang, W. Wu, F. Zhao, and G. M. Zhao, Phys. Rev. B **84**, 174440 (2011).

[13] Ò. Iglesias and A. Labarta, Phys. Rev. B **63**, 184416 (2001).

[14] A. M. Ferrenberg and D. P. Landau, Phys. Rev. B **44**, 5081 (1991).

[15] A. Lyberatos, D. Weller, G. J. Parker, and B. C. Stipe, J. Appl. Phys. **112**, 113915 (2012).

[16] K. Fabian, V. P. Shcherbakov, S. A. McEnroe, P. Robinson, and B. P. Burton, Geophys. J. Int. **202**, 1029 (2015).

[17] M. Mezard, G. Parisi, and M. A. Virasoro, *Spin Glass Theory and Beyond* (World Scientific, Singapore, 1987).

[18] K. Christensen and N. R. Moloney, *Complexity and Criticality* (Imperial College Press, London, 2005).

[19] P. J. Jensen, H. Dreyssé, and K. H. Bennemann, Surf. Sci. **269–270**, 627 (1992).

[20] S. Balay, S. Abhyankar, M. F. Adams, J. Brown, P. Brune, K. Buschelman, L. Dalcin, V. Eijkhout, D. Kaushik, M. G. Knepley, L. C. McInnes, W. D. Gropp, K. Rupp, B. F. Smith, S. Zampini, and H. Zhang, PETSc Users Manual, Tech. Rep. ANL-95/11 Rev 3.7 (Argonne National Laboratory, 2016).

[21] C. G. Shull, E. O. Wollan, and W. C. Koehler, Phys. Rev. **84**, 912 (1951).

[22] D. J. Dunlop and Ö. Özdemir, *Rock Magnetism: Fundamentals and Frontiers* (Cambridge University Press, Cambridge, 1997).

[23] GR. DIFF. INLASTIQUE DES NEUTRONS, J. Phys. Colloq. **32**, C1-1182 (1971).

[24] K. Fabian, V. P. Shcherbakov, and S. A. McEnroe, Geochem., Geophys., Geosyst. **14**, 947 (2013).

[25] V. P. Shcherbakov, K. Fabian, N. K. Sycheva, and S. A. McEnroe, Geophys. J. Int. **191**, 954 (2012).

[26] M. Uhl and B. Siberchicot, J. Phys.: Condens. Matter **7**, 4227 (1995).

[27] K. Levenberg, Quart. Appl. Math. **2**, 164 (1944).

[28] H. E. Stanley, *Introduction to Phase Transitions and Critical Phenomena* (Oxford University Press, Oxford, 1987).

[29] E. A. Velásquez, J. Mazo-Zuluaga, J. Restrepo, and Ò. Iglesias, Phys. Rev. B **83**, 184432 (2011).